Fusion Engineering and Design 200 (2024) 114106

Contents lists available at ScienceDirect

Fusion Engineering and Design

journal homepage: www.elsevier.com/locate/fusengdes

# Preliminary thermal and structural analyses on the parabolic mirror of the Multi-Beam Transmission Line of the DTT ECH system

A. Salvitti [a,*], A. Bruschi [b], G. Calabrò [a], F. Fanale [c,d], P. Fanelli [a], S. Garavaglia [b], F. Giorgetti [c,d], G. Granucci [b], A. Moro [b], P. Platania [b], A. Romano [c,d]

[a] Department of Economy, Engineering, Society and Business (DEIm), University of Tuscia, Viterbo, Italy
[b] Institute for Plasma Science and Technology – National Research Council of Italy, Milan, Italy
[c] ENEA, Fusion and Nuclear Safety Department, C.R. Frascati, Via E. Fermi 45, I-00044 Frascati (RM), Italy
[d] DTT S.C.a r.l., Via E. Fermi 45, I-00044 Frascati (RM), Italy

ARTICLE INFO

*Keywords:*
DTT
ECH
MBTL
Mirror
Thermo-structural analysis
Deformation

ABSTRACT

The Italian tokamak DTT (Divertor Tokamak Test) is a facility for research on nuclear fusion with the aim of investigating alternative power exhaust solutions to be exploited in the future DEMO fusion power plant. DTT foresees three additional heating systems to provide the plasma with sufficient power: Electron Cyclotron Heating (ECH) is the main one, with up to 32 MW installed. It consists of 4 clusters, each one composed of eight radio-frequency sources (gyrotrons) with their single-beam transmission lines, one quasi-optical Multi-Beam Transmission Line (MBTL) and eight independent launchers. The power produced by the source is transmitted quasi-optically through multiple reflections on metallic mirrors, the basic component of the transmission line, and then injected into the plasma.

In the MBTL the reflection of the eight microwave beams on the mirror surface leads to heating of its whole structure due to the absorbed fraction of the beam power (0.21–0.27 %) ascribed to the ohmic heating at the mirror surface. During the radio-frequency power pulse (100 s), the mirror temperature increases, generating deformations that could result in a loss of beam transmission efficiency. For this reason, these mirrors need to be carefully designed from thermal and structural points of view, to guarantee the required optical performances. In the present paper, a preliminary study concerning the design of the MBTL parabolic mirror, and its cooling is presented, resorting to a coupled thermal and structural finite element simulation. The preliminary analyses address a main objective: minimize the surface mirror temperatures and consequently the deformation associated with thermal expansion, to reduce the impact on beam transmission efficiency drop. Different design choices, namely materials, body thickness and cooling solutions, in terms of cooling channel shape and water flow, are discussed.

## 1. Introduction

In the research field of nuclear fusion, the Divertor Tokamak Test facility (DTT) [1] is an Italian project, aimed to investigate alternative power exhaust solutions under integrated physics and technical conditions that can be reliably extrapolated to the future nuclear fusion DEMOnstration power plant (DEMO) [2]. In DTT, to achieve a large value of the power crossing the boundary, an additional heating power of 45 MW must be provided to the plasma [3]. Three heating systems are selected for this purpose: Electron Cyclotron Heating (ECH), Ion Cyclotron Heating [4] and Neutral Beam Injection [5].

The ECH system architecture is based on 4 clusters, each one consists of 8 gyrotrons, the chosen Radio-Frequency (RF) source, one quasi-optical Transmission Line (TL) and 8 independent launchers [6].

The power produced by the RF sources is transmitted by a series of flat and focusing mirrors, enclosed in a metallic envelope under vacuum, and it is launched into the plasma by a pair of mirrors in the port plug for each launcher.

The gyrotron frequency is 170 GHz and produces a millimetre-wave beam of 1 MW of power. The quasi-optical TL is conceptually divided into three parts: the first and the third ones are Single-Beam Transmission Lines (SBTL), located close to the gyrotrons and preceding the

* Corresponding author.
*E-mail address:* alessandra.salvitti@unitus.it (A. Salvitti).

https://doi.org/10.1016/j.fusengdes.2023.114106
Received 29 May 2023; Received in revised form 8 December 2023; Accepted 11 December 2023
Available online 30 January 2024

launcher. The central part of the TL is a Multi-Beam Transmission Line (MBTL), most of which is located in a corridor between the gyrotron building and the torus hall. Its concept is the same of W7-X, where a quasi-optical system was adopted for the transmission line [7,8]. The DTT MBTL is composed of large focusing and plane Multi-Beam Mirrors (MBMs), each dedicated to the reflection of 8 beams. 8 MBMs, 4 focusing and 4 flat mirrors constitute the basic unit (Fig. 1) in the corridor.

The TL power handling requirements include the flexibility to increase the power up to 1.5 MW, considering a future upgrade of the gyrotron power [9]. The RF pulse is expected to be active for 100 s continuously with a repetition rate of one pulse per hour [9]. During a pulse, a fraction of 0.21–0.27 % of the incident power is absorbed by the mirror. As a natural consequence, the mirrors increase their temperature at each power pulse. Therefore, they must be cooled in order to avoid overheating and high deformations.

The following sections describe the preliminary design of the MBTL focusing mirror, which was optimized with the aid of thermal and structural Finite Element (FE) simulations.

The study includes the choice of materials, the geometrical design for both mirror and cooling channel, and the thermo-fluid dynamic water parameters.

The design is driven by the minimization of the mirror deformations, needed to guarantee high efficiency of beam transmission.

This requirement is strictly related to the minimization of temperature values and gradients as well.

### 1.1. Assumptions

The mirror under analysis is focusing, with a parabolic surface curvature and an elliptical outer frame.

Fig. 2 shows the geometric configuration with the minor and major radii of 380.0 mm and 537.4 mm, respectively. In particular, the minor dimension depends on the beam radius, as explained in [10]. The major dimension is determined by the beam incidence angle $(\theta_i = 45^\circ)$, and the parabolic surface of the mirror is given by a portion of a paraboloid of revolution. Specifically, it is defined by the parabola $y_G = x_G^2/(2\rho)$ at the off-axis radius $\rho$, where $Y_G$ and $X_G$ are the axes of the Global reference system and $\rho$ is defined as $\rho = \frac{F}{\cos^2\theta_i}$ [11], with the focal length of the mirror F = 2.85 m. The condition of $(\theta_i = 45^\circ)$ results in $\rho = 2F$.

During the 100 s of the pulse length, a MBM must simultaneously reflect on its surface 8 beams.

Ideally, at the input plane of the MBTL, the centres of the beams are disposed on the vertices of an octagon. Being the mirror non-planar but inclined at 45° and placed 5.7 m (2F) away from the input plane, the reflected beams are not covering an octagonal area, but rather a quasi-elliptical area (as shown in [9,10]).

Being inside a vacuum envelope, far from the plasma, the only load to which the mirror is subjected is the absorbed fraction of the microwave beams power. It is a surface load, defined by the Gaussian power distribution of the beams, with the size defined by the TL design, which is based on quasi-optical Gaussian beam propagation laws [11].

The incident power density per single beam is calculated as follows:

$$P_{inc} = P_0 \cdot e^{-2\left[\left(\frac{x_L}{w_x}\right)^2 + \left(\frac{y_L}{w_y}\right)^2\right]} \quad (1)$$

where the peak power density is:

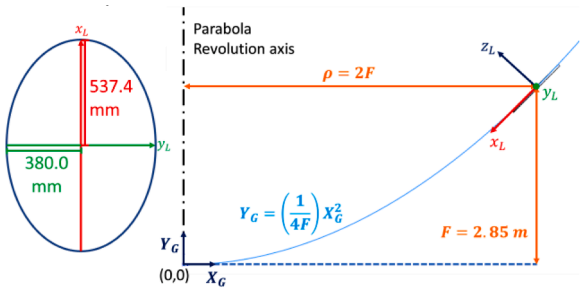


**Fig. 2.** Representation of the parabolic mirror features. On the left the elliptical shape with radii dimensions. On the right the representation of the parabola generating the mirror paraboloid surface. Subscripts L and G on the reference systems stand for "Local" and "Global".

$$P_0 = \frac{2Q}{w_x' w_y' \pi} \quad (2)$$

$Q$ is the total power of a single gyrotron beam ($Q = 1.5\ MW$ considering the maximum possible power unit).

The mirror local coordinates $x_L$ and $y_L$ (Fig. 2, left) are aligned with the major and minor mirror semi-axes, respectively, whilst $w_x'$ and $w_y'$ are the projected beam sizes on the $x_L$-$y_L$ plane.

The load is the absorbed power density on the mirror surface, calculated as:

$$P_{abs} = P_{inc} A \quad (3)$$

where A is the power absorption coefficient, evaluated considering the material resistivity at 30 °C, a mirror roughness factor of 1.3 [12] and the worst beam polarization in terms of ohmic losses on the reflective materials. An analysis with ohmic losses consistent with the mirror surface temperature is planned for the final cooling configuration, once completed.

The microwave power absorbed in the reflection of 8 beams is 25.2 kW in the case of copper and 32.4 kW in the case of the aluminium mirror surface.

In Table 1 the parameters for the load calculation are reported, where the values of $w_x'$ and $w_y'$ are the average sizes, representative of the 8 beams.

Fig. 3 represents the absorbed power density as a function of the coordinates $x_L$ and $y_L$.

### 1.2. Numerical modelling

The transient thermal analyses are aimed to simulate the variation of the temperature on the mirror during the RF pulse, but also during the time interval between pulses (3600 s), in which the mirror temperature

**Table 1**
Microwave load parameters.

| | $w_x'$ [m] | $w_y'$ [m] | $P_{abs\ MAX}$ [$MW/m^2$] | A |
|---|---|---|---|---|
| **Cu** | 0.15040 | 0.10635 | 0.14329 | 0.21 % |
| **Al** | 0.15040 | 0.10635 | 0.18422 | 0.27 % |

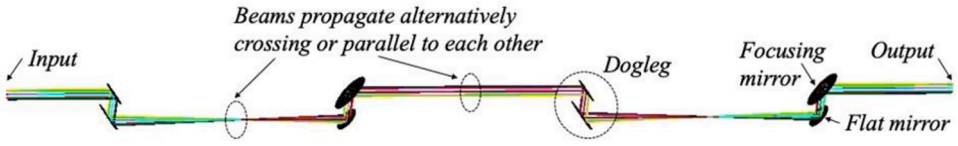


**Fig. 1.** Representation of the basic unit of a MBTL, with 8 reflecting mirrors (4 focusing and 4 flat mirrors). Figure from [9].

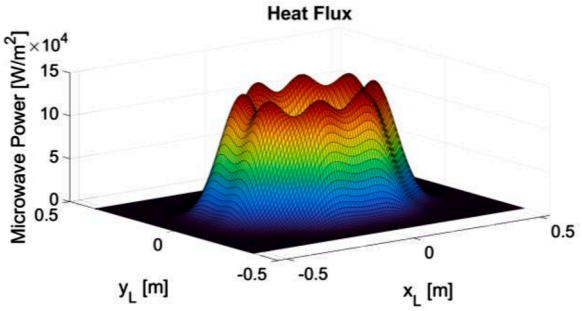


**Fig. 3.** 3D Representation of the absorbed power density distribution.

should return close to the initial value.

The theoretical approach for the thermal analysis is the same used for a mirror in the DTT launcher [13] in which the turbulent flow is treated with the empirical "Dittus-Boelter" formulation. For the refrigerant water, flowing in the cooling channel, the convection heat transfer coefficient (HTC) is considered uniform in space and constant in time, despite the performed analyses are transient. Nevertheless, this is a conservative approximation resulting in a small overestimation of the maximum temperature. Moreover, from the results it will be shown that the range of the water temperature is not too large, so the variability of the HTC, caused by the transient condition of the water, is limited.

ANSYS® [14] is the CAE software used for the simulations via both the Workbench interface and the APDL language.

The thermal FE approach exploits an ANSYS element type "FLUID116" to simulate mass and heat transport, and convection effects. This simulation approach simplifies the characterisation of the real fluid, losing detailed information on its fluid dynamics (for example, it does not consider centrifugal effects in non-rectilinear pipes), but still guaranteeing reliable temperature results.

The mesh models are mainly structured, and the elements used are mostly linear hexahedra. A mesh sensitivity analysis was performed on all models, which will be presented later, leading to high degree of refinement.

## 2. Definition of different mirror models

To find the best configuration that limits the deformations as much as possible, a comparison of different designs has been first performed. The models differ in both geometry and material. At the beginning, two simple designs were taken into account, to study the possibility to work in simplified conditions, realizing a cooling channel with a single turn. Then, two advanced cooling designs, with a double spiral configuration, were introduced, which could provide more relevant results in this type of application.

The first option considered for the material (as shown in [9]) is aluminium, which allows reducing weight and costs as well.

The second option is a Stainless-Steel (SS) mirror coupled with a copper layer. It is characterized by lower power to be dissipated thanks to the lower electrical resistivity of copper (resulting in lower ohmic losses), but on the other hand, it leads to a larger weight and lower thermal conduction in the bulk.

The two advanced options involve improving the cooling channel, by introducing the concept of a double spiral path, which increases the heat exchange area and allows for better temperature uniformity. The first application is on a SS mirror coupled with a copper layer (configuration similar to W7-X mirror [15]), whilst the second on a pure-copper mirror.

In the following sections, the models are presented more in detail.

### 2.1. Aluminium design (Elliptical channel)

The first design concerns an aluminium (Aluminium Alloy 6061-T6) mirror with a minimum thickness of 3 cm (the curvature of the paraboloid produces a variable thickness; the minimum is in the centre of the mirror).

Since copper is a noble metal and has a higher reduction potential than aluminium, in order to decrease the possibility of corrosion problems with water, the cooling channel is realized inside a copper plate, joined to the back surface of the aluminium mirror.

It is an elliptical plate of 50 cm x 40 cm (diameters) with a thickness of 2 cm. The cooling channel is a duct of elliptical shape with a circular cross-section of 1 cm in diameter. It is drawn on the ellipse containing the imprints of the beam centres. The geometry is visible in Fig. 4. The total weight of the mirror and the plate is ~ 87 kg.

### 2.2. SS-Cu design (Elliptical channel)

The second design foresees a minimum thickness of 3 cm (at the centre) with a SS bulk (2.5 cm of constant thickness) and an upper layer of copper with a minimum thickness of 0.5 cm (Fig. 5). The SS base is dug similarly to the copper plate of the aluminium mirror, but in this case, the channel has a semi-circular cross-section, being placed between the two materials. The position of the channel is translated closer to the reflection surface and consequently, near to the thermal load, considering the possibility to dig the channel into the SS surface and then add the copper layer by electroforming or other joining methods. To have approximately the same cross-section area as the previous case (circular section with 1 cm of diameter), it is necessary to build a semi-circular section with a diameter of 1.4 cm. This mirror has a total weight of 181 kg (55 kg Cu and 126 kg of SS).

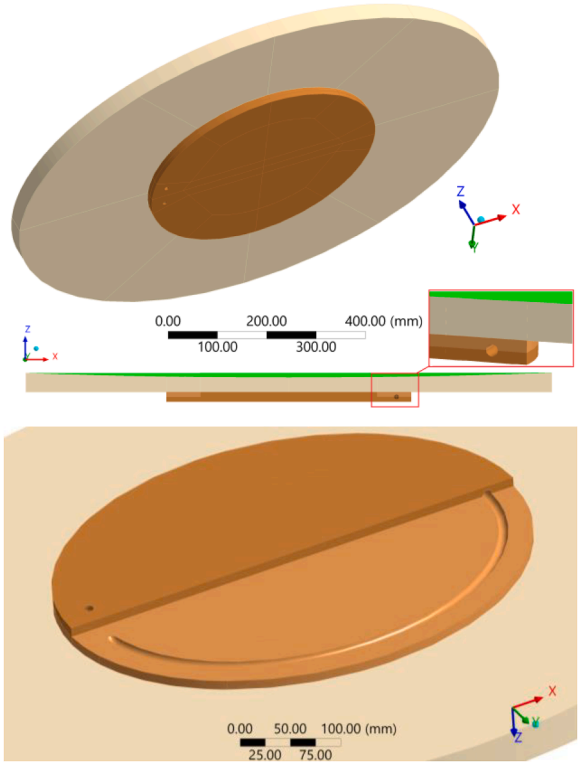


**Fig. 4.** Aluminium mirror geometry. (Top) General view. (Middle) Section view with the detail of the channel section. In green the reflective surface. (Bottom) Details of the dug elliptical plate. It is partially open to appreciate the channel.

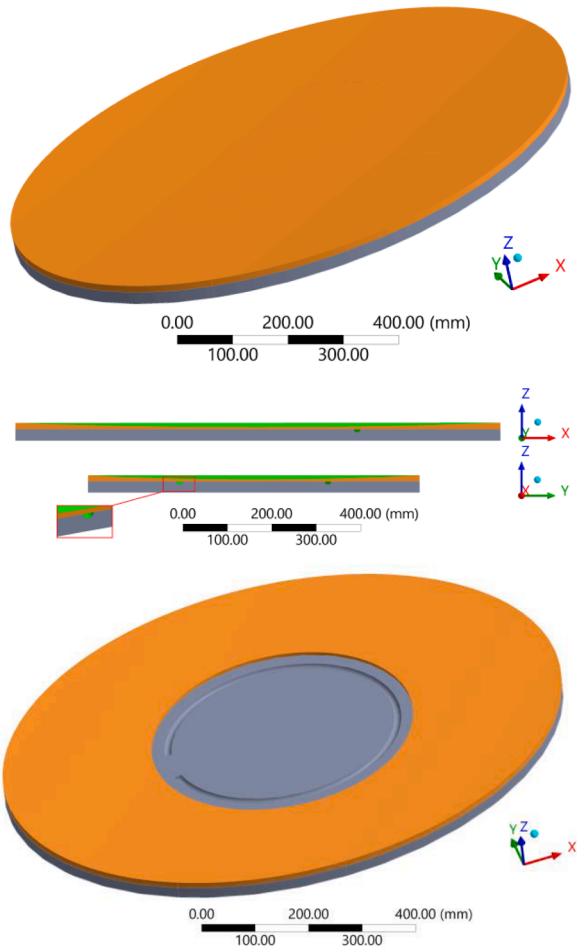


**Fig. 5.** SS-Cu mirror geometry. (Top) General View. (Middle) Section views (x-z, y-z planes). In green the reflective surface and the channel. (Bottom) View of the superior surface with the dug elliptical circuit. The cover layer is partially open to show the channel.

### 2.3. SS-Cu design (Spiral channel)

The third design considers a new configuration. It is proposed to try to: (1) decrease eventually high temperatures, (2) improve the cooling and (3) homogenize the temperatures.

To increase the cooling effectiveness, having a close contact to the whole reflective surface, it is possible to realize a spiral channel, as used for the steering mirror M2 of the ECH launcher [13] and widely studied for the TL mirrors of W7-X [15–17]. This could produce a more homogeneous distribution of the temperature and a decrement in the maximum values, pursuing all objectives (1), (2) and (3), provided that the channel covers a great part of the area of the mirror.

The concept of the spiral is interesting because it allows a more uniform distribution of heat across the mirror, bringing the water in contact with a larger area, and promoting heat exchange from the most heated to the less heated mirror regions. To this aim, the inlet of the channel is located near the maximum heat flux radius: so that the coldest water is in contact with the hottest zone of the mirror. From the inlet, two different spirals start, the first one towards the centre of the mirror and the second one towards the outside of the mirror, so the mass flow rate is divided into two channels (Fig. 6).

In this third design, the structure is composed of a SS base, dug with a semi-circular section channel, and covered by a parabolic layer of copper, as in the second design. In this case the thickness is reduced, to reduce the weight. The total minimum thickness is 2 cm, with a minimum thickness layer of 3 mm. The diameter of the semi-circular section

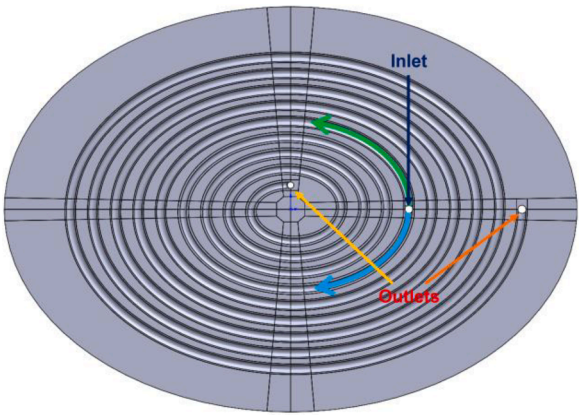


**Fig. 6.** Mirror with spiral cooling circuit geometry with hollowed-out channels and the holes of the inlet and the internal/external outlets.

is equal to the previous one: 1.4 cm.

The trajectory of the channel is an elongated spiral that follows the elliptical shape of the mirror. The spiral pitch is 3 cm for the minor axis and for the major axis 3 cm multiplied by the ratio between the ellipse radii. The angular range of the spiral is $3\pi - 20.5\pi$.

This mirror has a total weight of 122 kg (43 kg Cu and 79 kg of SS).

### 2.4. Copper design (Spiral channel)

The fourth design considers the double spiral concept, with the same dimensions and features of the third one, but in a pure-copper mirror. To pursue objectives (1), (2), (3) of Section 2.3, a pure-copper mirror could be better than the previous materials due to a higher thermal conductivity, lower thermal expansion coefficient (with respect to aluminium) and the possibility to use 3D printing. The con is the higher cost.

This mirror has a total weight of 132 kg.

## 3. Thermo-structural simulations, inputs, and results

Thermo-structural analyses are the basis on which the search for the best model is developed. In the following sections, the main results for all the simulations are shown, starting from the input conditions. For each design proposed in Section 2, the transient thermal and static structural simulations are given.

The transient analyses are carried out on three pulses (10,800 s), divided into 114 time-steps, finer (10 steps) during each RF pulse (100 s long). The thermal load only is active for 100 s and three times in the whole simulation.

The input parameters of the thermal analysis are:

- volumetric flow rate: $\dot{V} = 20\ l/min$
- water inlet temperature $T_{water\ (inlet)} = 30°C$
  (first attempt value: temperature easily available in every season to not create problems of condensation)
- water inlet pressure: $p_{water\ (inlet)} = 10\ bar$ (conservative value considering possible high pressure drops in the whole circuit)
- heat transfer coefficient: defined for each configuration.

In this preliminary design, the structural analyses are performed with simplified boundary conditions. In order to decrease the computational effort, it was decided to analyse a steady-state structural condition at a given time, corresponding to a specific thermal condition. A transient structural analysis will be considered with the most promising mirror design.

Hereafter the structural simulation will concern the time instant related to the highest temperature, occurring at the end of the third shot (7300 s).

In the static structural analysis, the loads are:

- the temperature distribution at 7300 s
- the water pressure on the channel walls (10 bar conservatively constant)
- the forces at the inlet and the outlet that simulate the continuity of the flow.

Concerning the constraints, a free displacement is simulated. As the load is quasi-symmetrical with respect to the mirror centre, it is possible to assume a null displacement in the directions normal to the symmetry planes and a null displacement on the vertical direction of the centre of the back surface (indeed, the real support could be connected to the mirror in the central back area). The equivalent support will be improved subsequently, considering a more realistic condition.

In this paper, gravitational effects, which have a non-negligible impact on the shape of the mirror, will not be considered, in order to assess only the effects related to thermal load. In a future detailed design, they will be added, and if necessary, the possibility of compensating them in the original shape of the mirror will be considered.

### 3.1. Aluminium design (Elliptical channel) thermo-structural results

The input parameters of the thermal analysis have already been reported. Only the HTC needs to be specified for each configuration:

- heat transfer coefficient: $h \cong 17000\ W/(m^2K)$, constant, calculated considering the water properties at $T_{water\ (inlet)}$.
- The Reynolds number is $\sim$ 53000, a value that confirms fully turbulent flow inside the channel.

Fig. 7 reports the first simulation result of the design of Section 2.1: the temperature distribution at the end of the third pulse, at 7300 s (the distributions at the end of the first and second pulses are the same as the third, so they are not shown). The maximum temperature reached on the mirror is 116.2 °C, an acceptable value in this kind of application (as seen in [13]), but it must be considered in relation to the thermal expansion effect. For this reason, a structural analysis is essential.

The water outlet temperature at the end of the 3rd pulse reaches 41 °C, still low, and its properties change little enough to consider the HTC constant.

The maximum heat power absorbed by the water during the simulation is $Q = \dot{m}c_p\Delta T_{water} \cong 15.25\ kW$, $\sim$ 47 % of the total absorbed power (Section 1.1).

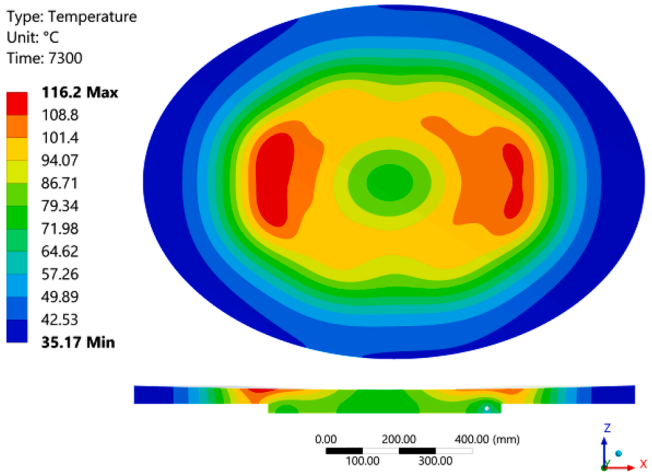


**Fig. 7.** Aluminium mirror design: (Top) Contour plot of the temperature distribution at the end of the third pulse, front view. (Bottom) Temperature distribution on the section view (x-z plane).

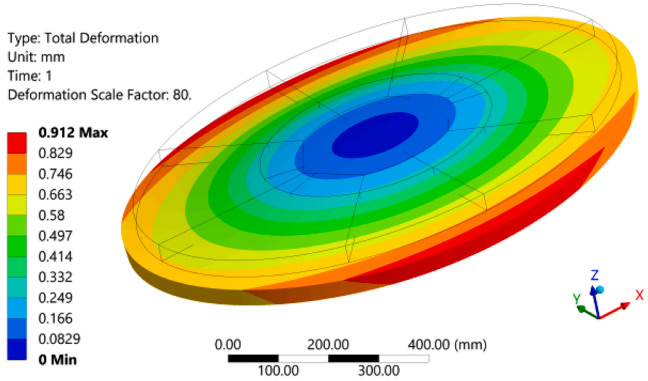


**Fig. 8.** Contour plot of the total deformation of the aluminium mirror design. Deformation scale factor (x80).

The time evolution of the maximum mirror surface temperature will be reported in Section 3.5.

Considering the structural constraints mentioned above, a static structural analysis (at 7300 s) is carried out. Fig. 8 shows the contour plot of the total deformation.

As visible in Fig. 8 the maximum total deformation is 0.912 mm. The directional deformations out of the reflection plane are the most critical for the propagation efficiency of the beam, so the most important to be analysed. The trends and the maximum values of the Z-directional deformation (out of the mirror plane) in the main axes (on the superior surface) of the mirror will be reported in Section 3.5.

### 3.2. SS-Cu design (Elliptical channel) thermo-structural results

The input parameters of the thermal analysis have already been reported. Only the HTC is here different with respect to the previous design due to the small change in the cross-section area:

- heat transfer coefficient: $h \cong 17600\ W/(m^2K)$, constant, calculated considering the water properties at $T_{water\ (inlet)}$.
- The Reynolds number is $\sim$ 46000, a value that confirms fully turbulent flow inside the channel.

The reflective material of the design of Section 2.2 is different from before, as reported in Table 1. The heat flux distribution changes and the peak is lower.

Fig. 9 shows the temperature distribution at the end of the third

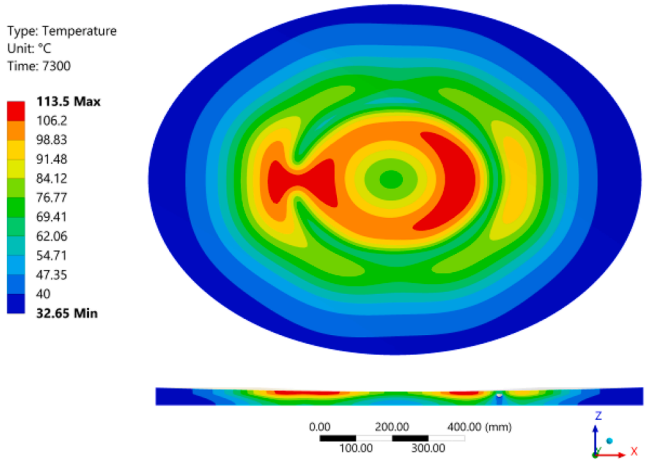


**Fig. 9.** SS-Cu (Elliptical) mirror design: (Top) Contour plot of the temperature distribution at the end of the third pulse, front view. (Bottom) Temperature distribution on the section view (x-z plane).

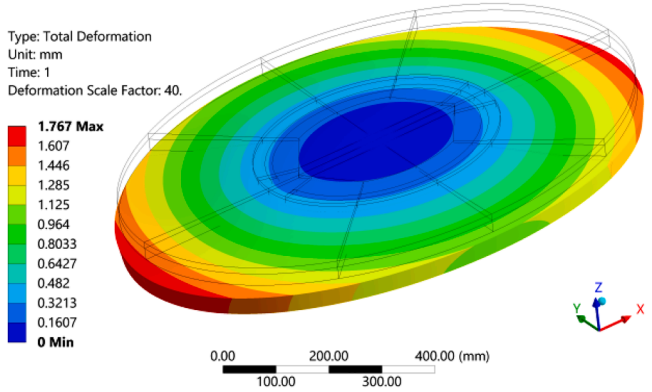


**Fig. 10.** Contour plot of the total deformation of the SS-Cu (Elliptical) mirror design. Deformation scale factor (x40).

pulse. The pattern is different from the previous one, but the maximum temperature is 113.5 °C, only 3 °C lower than the previous case. The channel contour and the effect of the cooling along the path is well visible.

The difference with the previous case is due to the change of the materials and the different thermal behaviour. As already mentioned, the thermal conductivity of the SS is lower than the one of the aluminium or copper, so the back surface remains colder and heat conduction gets worse, but the position of the channel, close to the load, still allows for lower maximum temperature. Maintaining the same conditions and moving the channel closer to the rear surface would increase the temperatures.

In this case, the maximum water outlet temperature is 38.1 °C (at 7300 s). The water temperature difference is low, and the maximum heat power absorbed by the water during the simulation is $Q = \dot{m}c_p\Delta T_{water} \cong 11.2\ kW$,~ 44 % of the total absorbed power. It is lower in absolute value than in the previous case, but similar in percentage, because the total power is lower for copper (Section 1.1).

The time evolution of the maximum temperature of the copper mirror will be reported in Section 3.5.

As done previously, a static structural analysis has been carried out with the thermal condition at 7300 s, with unchanged boundary conditions.

The first important result is that the maximum total deformation increases by ~ 94 % compared to the aluminium case, up to 1.767 mm (Fig. 10).

The trends and the maximum values of the Z-directional deformations for the major and minor axes of the superior surface will be reported in Section 3.5.

### 3.3. SS-Cu design (Spiral channel) thermo-structural results

The analysis of the designs of Sections 2.3 and 2.4 considers the same diameter and the same volumetric flow rate (10 l/min) for internal and external spirals. The heat transfer coefficient is $h \cong 10000\ W/(m^2K)$, with $Re \cong 23100$.

The results of the thermal analysis of the third design of the SS-Cu mirror with spiral channel, at the end of the third pulse (7300 s), are visible in Fig. 11.

The maximum surface temperature is remarkably decreased, up to 67.6 °C. The temperature distribution is also more uniform, resulting in a lower maximum gradient. The water outlet temperature in the inner spiral reaches a value of 43 °C, while in the external spiral the maximum value is 49 °C, which is not reached at the outlet because, during the last round, the heat exchange changes and the water heats the outer edge of the mirror, which remains colder. This result is useful to better even out the temperature over the mirror, reducing the temperature gradients.

The maximum absorbed thermal power by the water during the

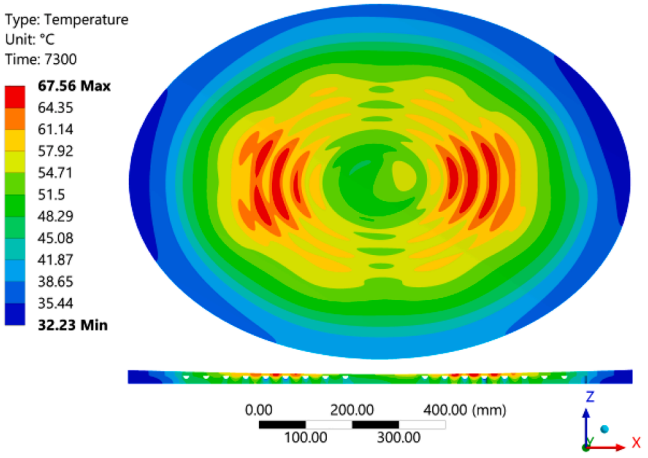


**Fig. 11.** SS-Cu (Spiral) mirror: (Top) Contour plot of the temperature distribution at the end of the third pulse, front view. (Bottom) Temperature distribution on the section view (x-z plane).

transient is $Q = \dot{m}c_p\Delta T_{water} \cong 21.9\ kW$, ~ 87 % of the total absorbed power (Section 1.1). This value is much higher than in previous configurations because, in this design, the cooling system is more effective, for the reason seen in Section 2.3.

The time evolution of the maximum temperature of the copper mirror will be reported in Section 3.5.

From here on, a more realistic constraint in structural analysis is considered.

With the hypothesis of a spherical joint to sustain the mirror at the centre of the back surface, new constraints are implemented in the simulations, as visible in Fig. 12.

The back central zone of the mirror has a compression-only support (in blue in Fig. 12), the central orthogonal faces are blocked to move in their normal direction (orange and green reference in Fig. 12) and the back centre is blocked in Z-direction (red reference in Fig. 12).

The maximum total deformation of the SS-Cu (spiral) mirror (at 7300 s) is 0.866 mm, and the contour plot is visible in Fig. 13.

With respect to the second design, the remarkable decrease in maximum $\Delta T$ across the mirror (56 %), leads to a 51 % decrease in maximum total deformation. However, this value is only 5 % lower than the result of the first design.

The trends and the maximum values of the Z-directional deformation in the main axes of the mirror will be reported in Section 3.5.

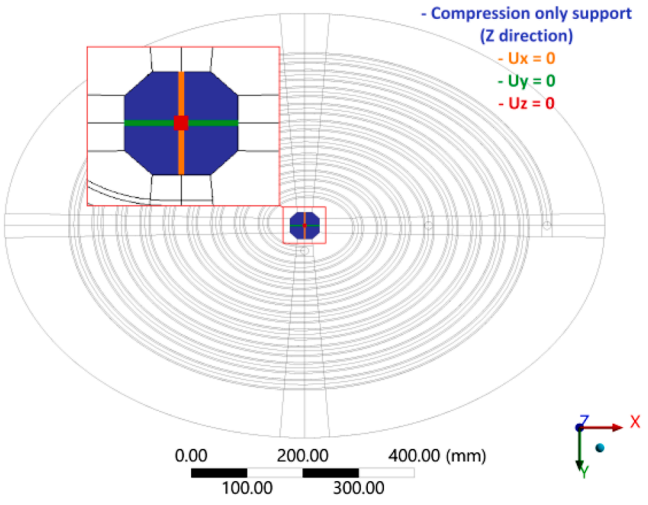


**Fig. 12.** Structural constraints of the Mirror with spiral cooling circuit.

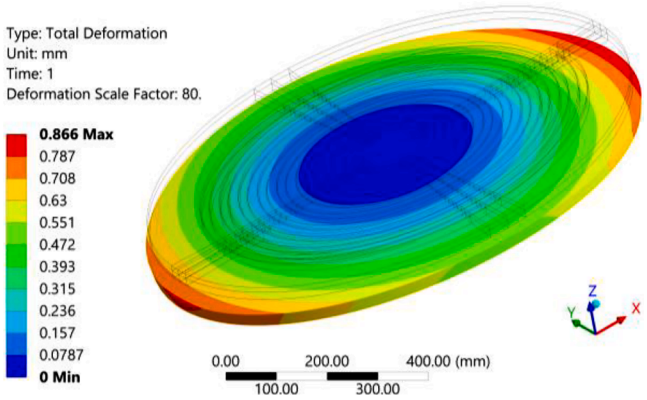


**Fig. 13.** Contour plot of the total deformation of the SS-Cu (spiral) mirror design. Deformation scale factor (x80).

### 3.4. Copper design (Spiral channel) thermo-structural results

The results of the thermal analysis of the fourth design of the pure copper mirror, at the end of the third pulse (7300 s), are visible in Fig. 14.

The maximum surface temperature is 55.1 °C, ~12 °C lower than the previous result. Fig. 15 allows to better appreciate the more uniform temperature, using the same scale of the third design. In this case, not only the maximum value is lower, but also the minimum value is higher, and this leads to a maximum gradient $\Delta T$ of 17 °C, against the previous one of 35 °C.

The water reaches the same condition, because there are no differences in the thermodynamic features, and the absorbed thermal power is the same.

The maximum total deformation of the copper mirror (at 7300 s) is reduced to 0.144 mm, and the contour plot is visible in Fig. 16.

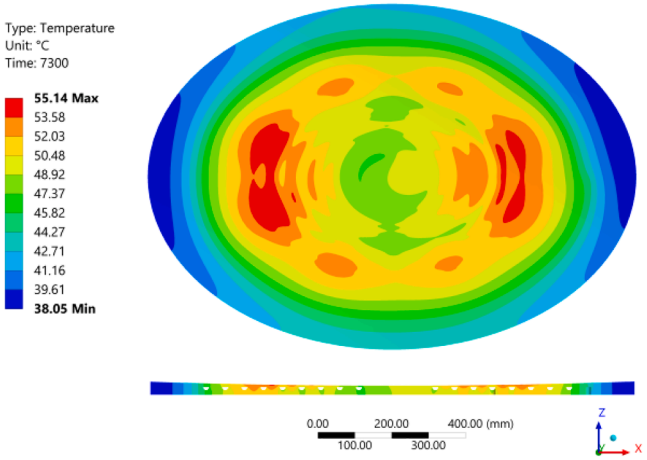


**Fig. 14.** Copper mirror: (Top) Contour plot of the temperature distribution at the end of the third pulse, front view. (Bottom) Temperature distribution on the section view (x-z plane).

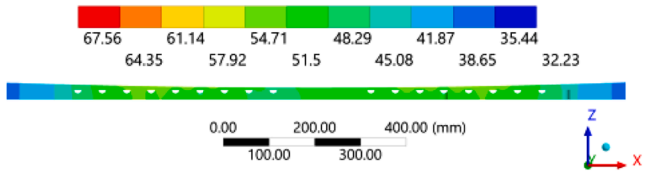


**Fig. 15.** Copper mirror: contour plot of the temperature distribution on the section view with the scale of the previous case.

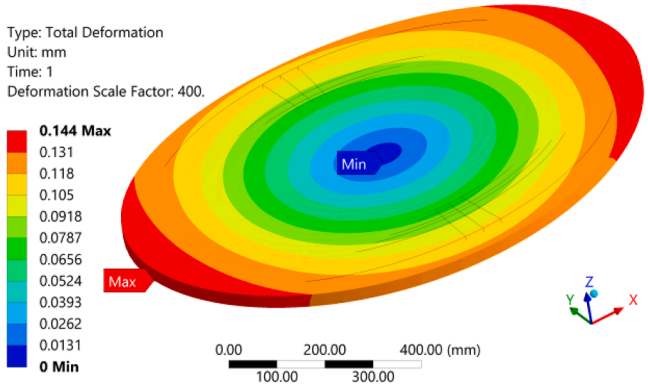


**Fig. 16.** Contour plot of the total deformation of the copper mirror design. Deformation scale factor (x400).

The large temperature drop leads to a significant decrease in the deformation. The maximum total deformation at the end of the pulse is about 83 % lower than the SS-Cu (spiral) result.

The trends and the maximum values of the Z-directional deformation in the main axes of the mirror will be reported in Section 3.5.

### 3.5. Comparison of the thermo-structural results

In this section, a comparison of the results of the four designs is illustrated.

Table 2 reports the main results in temperature and the Fig. 17 shows the time evolution of the maximum mirror surface temperature for the four configurations. The trends are pairwise similar in two aspects: the reached peak and the cooling rate. Both aspects are related to the channel characteristic. The elliptical channel leads to higher peaks and slower cooling (blue and grey trends), while the spiral channel to lower peaks and faster cooling (green and orange trends). In particular, the fourth design has a peak temperature reduced by ~ 52 % compared to the first configuration. This important improvement in the temperature distribution is certainly positive for the structural results.

Furthermore, in the first and second designs, the temperature after 1 h returns close to the initial condition, but not equal and they do not reach steady state before the next pulse. However, the maximum temperature rise at the end of each pulse is very low (~0.1 °C). In the third and fourth designs, the mirror recovers the initial condition before the next pulse, reaching the steady state 1100 s after the end of the pulse for the SS-Cu mirror and 700 s for the Cu mirror. Thus, it appears unnecessary to evaluate the thermal performance over three pulses, because one pulse is sufficient.

The Z-directional deformation maximum values in the major and minor axes of the superior layer of the mirror are reported in Table 3, in addition to the maximum value of the total deformation. In Fig. 18 the trends of the Z-directional deformations are shown for the main axes. The comparison of the four configurations shows that the design in SS-Cu (Elliptical) is the worst solution, the design in SS-Cu (Spiral), despite the improvement of the cooling and better thermal results, does not have a good structural performance, as opposed to the pure copper mirror. The main reason is the low thermal conductivity of the SS, which results in poor heat transfer within the structure and between successive

**Table 2**
Main temperature results of the four designs.

| Mirror 7300 s | AL Elliptical channel | SS-Cu Elliptical channel | SS-Cu Spiral channel | Cu Spiral channel |
|---|---|---|---|---|
| **Max T mirror** [°C] | 116.2 | 113.5 | 67.56 | 55.14 |
| **Max T water** [°C] | 41 | 38 | 43 int<br>49 ext | 43 int<br>49 ext |

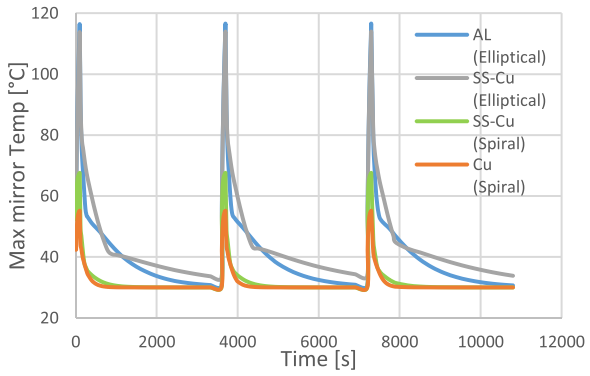


**Fig. 17.** Evolution of the maximum mirror temperature over time for the four design configurations considered.

**Table 3**
Maximum values of the total deformation and the Z-directional deformation on the major and minor axes of the four designs.

| Mirror | AL Elliptical channel | SS-Cu Elliptical channel | SS-Cu Spiral channel | Cu Spiral channel |
|---|---|---|---|---|
| **Max TOT def [mm]** | 0.912 | 1.767 | 0.866 | 0.144 |
| **Max Z def MAJOR axis [mm]** | -0.568 | -1.744 | -0.851 | 0.037 |
| **Max Z def MINOR axis [mm]** | -0.815 | -1.091 | -0.523 | -0.031 |

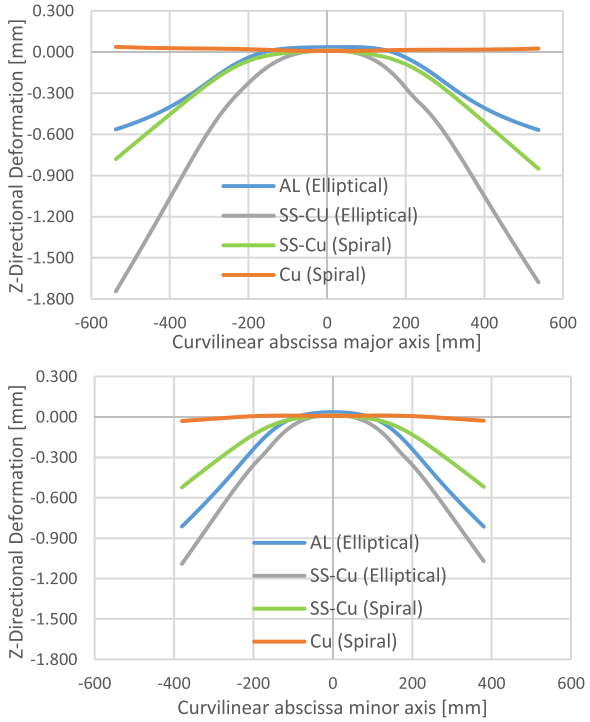


**Fig. 18.** Comparison of the Z deformation on major (top) and minor (bottom) axes between the four designs.

turns of the spiral, which is much less evident in copper. Reducing the pitch of the spiral (increasing the spiral range) can improve heat transfer and thus temperature distribution.

The pure copper mirror seems to be the best option. Not only the maximum total deformation decreases by 83 % in the pure copper mirror, but the maximum value of the Z-directional deformation decreases by 96 % on the major axis and 94 % on the minor axis (compared with SS-Cu (Spiral)).

The difference is that the deformation of the copper mirror on the major axis is positive contrary to the previous cases.

The copper mirror turns out to be the most suitable solution, certainly not free of charge. To achieve this, it was essential to consider a more complex cooling system and a heavier (more expensive) material.

## 4. Optimization of the mirror performance

Having found the best solution in the copper mirror design, as shown in Section 3, some features are then optimised.

### 4.1. *Effect of the mirror thickness*

The first optimization concerns the thickness. Pursuing the objective of reducing the deformations, different thickness values of the layer (3;4;5 mm) and of the mirror (1.5;2 cm) are studied.

The first solution of the copper mirror foresees a total thickness of 2 cm, with a minimum thickness for the layer of 3 mm. A parametric analysis for the different cases is executed. The results of the comparison are reported in Table 4 and the graphs of Fig. 19.

From the maximum values of the total deformation reported in Table 4, it is worth noting that the solution using 1.5 cm thickness is worse than 2 cm, regardless of layer thickness: less material allows a reduction of the weight of the structure, but it also reduces the stiffness, so the mirror becomes more prone to deformations.

**Table 4**
Comparison of the maximum values of total deformation and Z-directional deformation between five configurations of the copper mirror.

| | 2 *cm* 3 *mm* | 2 *cm* 4 *mm* | 2 *cm* 5 *mm* | 1.5 *cm* 3 *mm* | 1.5 *cm* 5 *mm* |
|---|---|---|---|---|---|
| **Max TOTdef [mm]** | 0.144 | 0.145 | 0.145 | 0.154 | 0.155 |
| **Max Z def Major axis [mm]** | 0.037 | 0.017 | 0.016 | 0.039 | 0.019 |
| **Max Z def Minor axis [mm]** | -0.031 | -0.043 | -0.051 | -0.044 | -0.064 |

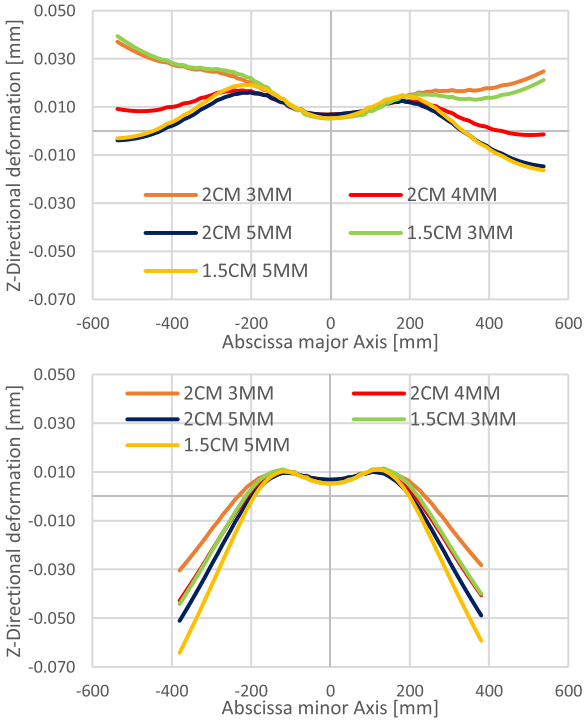


**Fig. 19.** Comparison of the Z deformation along major (top) and minor (bottom) axes between the five configurations of the copper mirror.

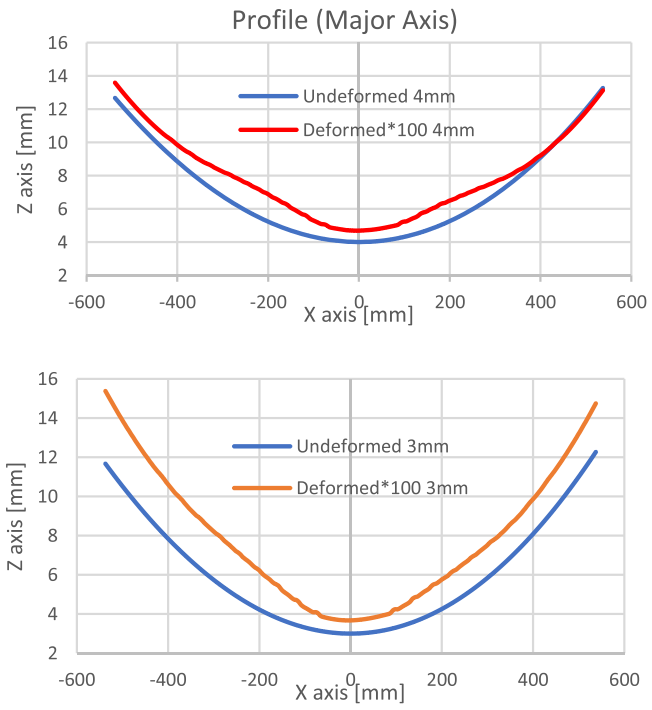


**Fig. 20.** Parabolic profile on the major axis in undeformed condition (blue trends) and deformed condition (scaled x100 in red and orange trends) for the case 4 mm (top) and 3mm (bottom).

The choice among the layer thickness (3 mm, 4 mm, or 5 mm) is not trivial. The 5 mm case seems to be better considering z-deformations on the major axis, but the 3 mm one exhibits lower deformation along the minor axis. The solution of 4 mm presents intermediate values of the maximum Z-directional deformations.

To individuate the final choice, it is useful to refer to Fig. 19, reporting the trends of Z-directional deformations on two main axes for all the configurations and Fig. 20, reporting the parabolic profile on the major axis in the deformed and undeformed conditions, for the cases with 4 mm and 3 mm layer thickness.

From Fig. 19, it is noteworthy that the trend for 4 mm case deformation is in the middle of the previous two. It produces a more homogeneous deformation in the major axis. From Fig. 20 the 3 mm case seems to be better in the central area where the beams reflect, but the total curvature increases more than the 4 mm case, affecting the focussing effect of the bundle of the 8 beams. So, the option with 2 cm bulk and 4 mm layer is chosen as the best solution.

### 4.2. Hydraulic flow balancing

As reported in Section 3.3, the mass flow rate is equal for both spirals internal and external. This leads to different pressure drops because the spiral lengths are not equal. With regard to the future installation of the cooling circuit, in order to avoid the use of intermediate valves or pumps, the system must be designed to have the same pressure drops. For this purpose, the following conditions must be satisfied simultaneously:

- Equal $\Delta P$ for internal and external spirals (evaluated for straight tubes and multiplied by a corrective factor of 1.5)
- $\Delta P = 1\ bar$ (arbitrary choice inside the range of 4 bar, compatible with DTT water cooling system)
- $\dot{V}_{tot} = \dot{V}_{int} + \dot{V}_{ext}$ (flow rate in the internal and external spiral, respectively)
- $\dot{V}_{tot} \cong 20\ l/min$

**Table 5**
Values of the channel diameters and velocities related to specific volumetric flow rates.

| $\dot{V}_{int}[l/\min]$ | $d_{int}[m]$ | $v_{int}[m/s]$ | $d_{ext}[m]$ | $v_{ext}[m/s]$ |
|---|---|---|---|---|
| **4** | 0.0084 | 2.4 | 0.0177 | 2.2 |
| **6** | 0.0098 | 2.6 | 0.0168 | 2.1 |
| **8** | 0.0109 | 2.8 | 0.0159 | 2.0 |
| **10** | 0.0119 | 3.0 | 0.0149 | 1.9 |
| **12** | 0.0127 | 3.2 | 0.0137 | 1.8 |
| **14** | 0.0135 | 3.3 | 0.0123 | 1.7 |
| **16** | 0.0142 | 3.4 | 0.0105 | 1.5 |

The system is solved by setting an array of internal mass flow rates (Table 5) and finding for each value a couple of internal and external diameters (consequently the external mass flow rate), which guarantee equal pressure drops.

In order to choose the optimal pair of diameters, seven thermal simulations, corresponding to the cases reported in Table 5, are carried out, without changing the geometry of the mirror (the diameters of the spirals), but using a reference geometry (2 cm - 5 mm) with $d_{int} = d_{ext} = 1.4\ cm$) and applying adaptive HTCs, calculated as follows:

$$h_{fem} = h_{eff} \cdot \frac{A_{side_{eff}}}{A_{side_{fem}}} \tag{4}$$

where $h_{fem}$ is the fictitious HTC to be used with the reference geometry, $h_{eff}$ is the effective HTC (calculated analytically with the correct diameters), $A_{side_{eff}}$ is the convection area of the effective geometry and $A_{side_{fem}}$ of the reference geometry.

The results of these thermal simulations are visible in Fig. 21, where the maximum $\Delta T$, the $T_{average}$ and $T_{max}$ of the mirror are plotted.

The choice of the pair of diameters is driven by the goal to minimize the temperatures. The lowest values are related to an internal flow rate of ~10 l/min.

The pair of diameters corresponding to this value of flow rate is approximatively $d_{int} = 12\ mm$, $d_{ext} = 15\ mm$. Such approximation leads to a $\dot{V}_{int} \cong 10.279\ l/min$ and $\dot{V}_{ext} \cong 10.280\ l/min$.

### 4.3. Complete thermal and structural analysis

Once all the studies and the comparisons have been executed, having the final design in geometry and material, the chosen thickness values and the hydraulic condition, it is useful to carry out a complete analysis. It concerns a coupled transient thermo-structural simulation, analysing the mirror temperature and deformation due to the heat flux and out of the loaded condition. The time evolution of the deformation will be thus analysed. The total analysis time is 300 s, considering one pulse only, as explained in the results of Section 3.5. The thermal load is active in the range of 10 s–110 s, to have stable conditions in the first 10 s.

Considering the final geometry (2 cm–4 mm) (Fig. 22), a structured mesh is realized, as visible in Fig. 23.

The thermodynamic parameters and values are:

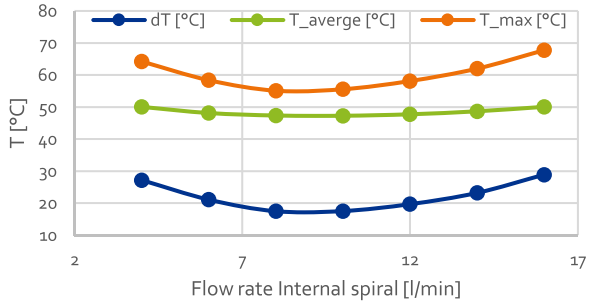


**Fig. 21.** Comparison of the results of the 7 sets of values $\dot{V}_{int}, d_{int}, d_{ext}$.


**Fig. 22.** Copper mirror (2 cm–4 mm) geometry: section view of half mirror.

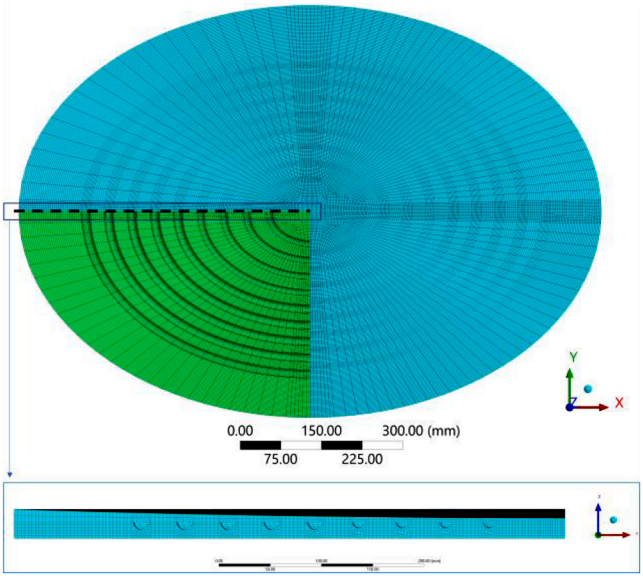


**Fig. 23.** (Top) Mesh of the (2 cm–4 mm) version of the copper mirror. In the bottom left corner, the detail of the mesh of the bulk with the channel is visible. (Bottom) Section view of half mirror.

- volumetric flow rate: $\dot{V}_{int} = 10.279\ l/min$, $\dot{V}_{ext} = 10.280\ l/min$
- water inlet temperature $T_{water\ (inlet)} = 30°C$
- water inlet pressure: $p_{water\ (inlet)} = 10\ bar$
- heat transfer coefficient:
  $h_{int} \cong 14000 \frac{W}{m^2K}$, $h_{ext} \cong 9000 \frac{W}{m^2K}$, with
  $(Re_{int} \cong 28000)$, $(Re_{ext} \cong 22000)$.
  HTCs constant, calculated considering the water properties at $T_{water\ (inlet)}$.

The boundary conditions of the structural analysis are the same as previously defined:

- temperature field
- channel internal pressure (10 bar)
- forces at the inlet and outlets for flow continuity
- support constraint (Fig. 12).

The results at the end time of the RF pulse are visible in Fig. 24.

The maximum surface temperature of the mirror over time is 54.97 °C. The water temperature reaches the value of 48.5 °C in the external spiral, whilst 43.8 °C in the internal spiral.

Figs. 25 and 26 show the contour plots of the total deformation at two different times, 44 s and 110 s, respectively. In the graph of Fig. 27, the maximum total deformation and maximum temperature over time are plotted, while Fig. 28 plots the maximum and minimum Z-directional deformation over time along the major and minor axes.

It is possible to observe that the total deformation is higher at 44 s (i.e. 34 s after the pulse start) than at the end of the shot (110 s, namely 100 s after the pulse start). The deformation value is 0.177 mm at 44 s versus 0.140 mm at 110 s. The temperature gradient across the thickness around 44 s is higher than that at the end time.

As visible from Fig. 28 the main difference between these instants is the deformation out of the mirror plane.

At 44 s the Z components are much higher than those at 110 s (see

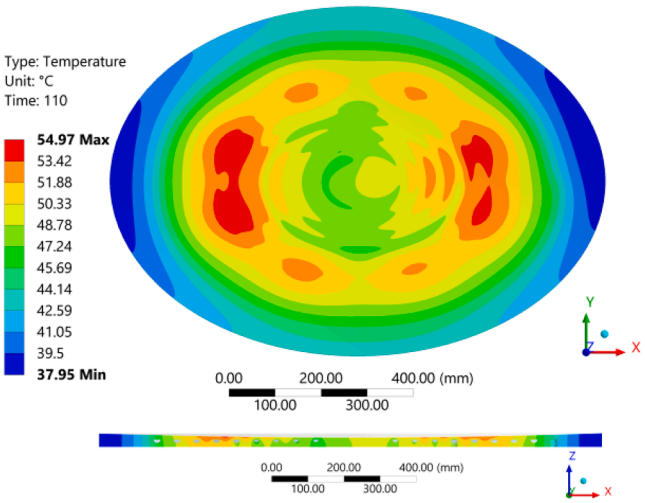


**Fig. 24.** Contour plot of the temperature at the end of the pulse in the latest version of the copper mirror: (top) frontal view, (bottom) section view (x-z plane).

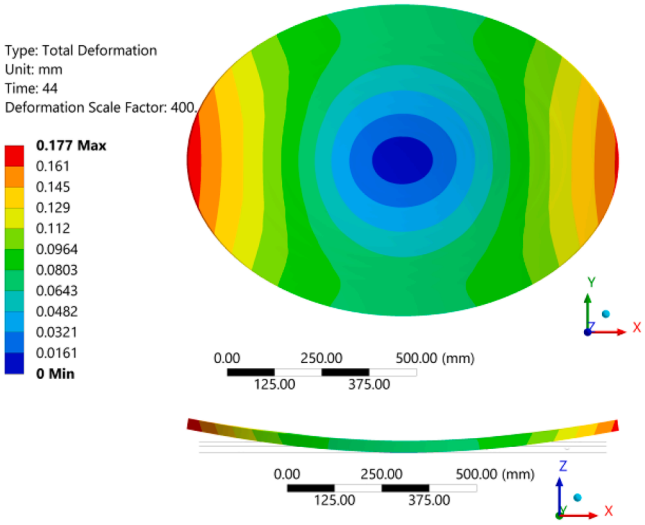


**Fig. 25.** Contour plot of the total deformation at 44s in the last version of the copper mirror: (top) frontal view, (bottom) side view. Deformation scale factor: x400.

also Fig. 28), where most of the total deformation is given by the X and Y components. Indeed, looking at Fig. 26 the deformation out of the mirror plane is lower than the expansion on the mirror plane. The black ellipse in Fig. 26 shows the undeformed mirror.

Looking at the first instants (~1.5 s from the start of the pulse) in Fig. 27, despite the low temperatures, the distribution of the temperatures produces a fast increment of the deformations. As visible in Fig. 28, this kind of deformation is in the opposite direction with respect to the one occurring at 44 s. Indeed, the Z-directional deformation at ~11.5 s is negative, whilst at 44 s it is positive. Therefore, considering this kind of results, not only the deformation at 110 s needs to be verified with electromagnetic codes, in order to study beam deflection, but also the mirror deformation at 44 s, which seems to be more effective, mainly due to the deformation out of the mirror plane.

Looking at Fig. 27, it is worth noting that an even higher total deformation is recorded around 150 s, but what happens after the 110 s is of little interest from the optical point of view. Indeed, at 150 s the impulse has already been interrupted, so these deformations do not affect the transmission efficiency of the beams.

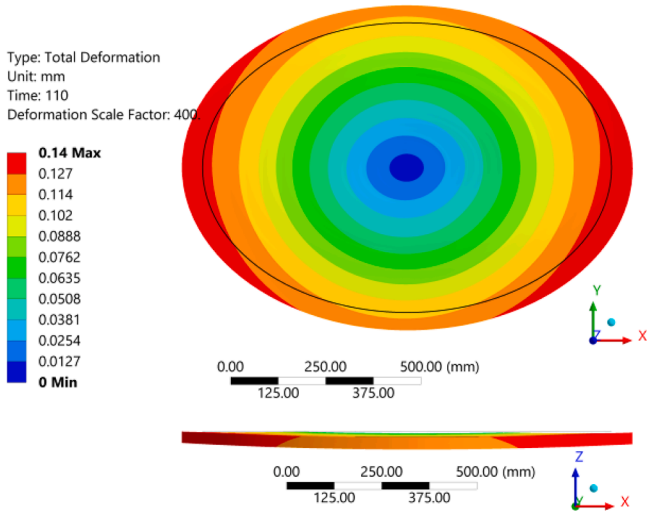


**Fig. 26.** Contour plot of the total deformation at 110s in the last version of the copper mirror: (top) frontal view, (bottom) side view. Deformation scale factor: x400.

From a structural point of view, the deformations associated with these thermal loads do not create problems for the system either during the impulse or afterwards.

Finally, Fig. 27 shows that after 300 s the temperatures return close to the initial conditions, as do the deformations. At the end of a duty cycle, lasting 1 h, the mirror temperature will have completely recovered to the initial conditions and its profile as well.

## 5. Conclusions

In this paper, a comparison of different parabolic mirror designs of the DTT ECH Multi-Beam Transmission Line was presented. The four configurations analysed include an aluminium and copper mirror (first case), a stainless-steel and copper mirror (second and third cases) and a pure copper mirror (fourth case). Different cooling options were studied: two simple designs with an "elliptical channel" for the first and second cases, and two advanced designs with a double "spiral channel" for the third and fourth cases. Thermo-structural simulations were carried out to evaluate the best option from a thermal and structural point of view. The study led to identify the pure copper mirror with "spiral channel" as the best configuration, which was optimized in the thickness and the hydraulic parameters.

It involves a copper mirror with a bulk dug by a cooling channel in the shape of a double spiral, with the addition of a cover layer. The minimum total thickness of the mirror is 2 cm, including 4 mm (minimum thickness) of the cover layer. The inlet of the cooling channel is located on the major axis, in correspondence with the peak of the heat flux hitting the mirror. Two outlets are foreseen, because the circuit is divided into two channels, one towards the centre of the mirror and one towards the external edge, to simultaneously cool two different areas of the mirror. Considering an inlet water temperature of 30 °C and a mass flow rate of ~ 10 l/min for both spirals, the maximum temperature on the mirror, during the 100 s of the pulse, is ~55 °C, recorded at the end

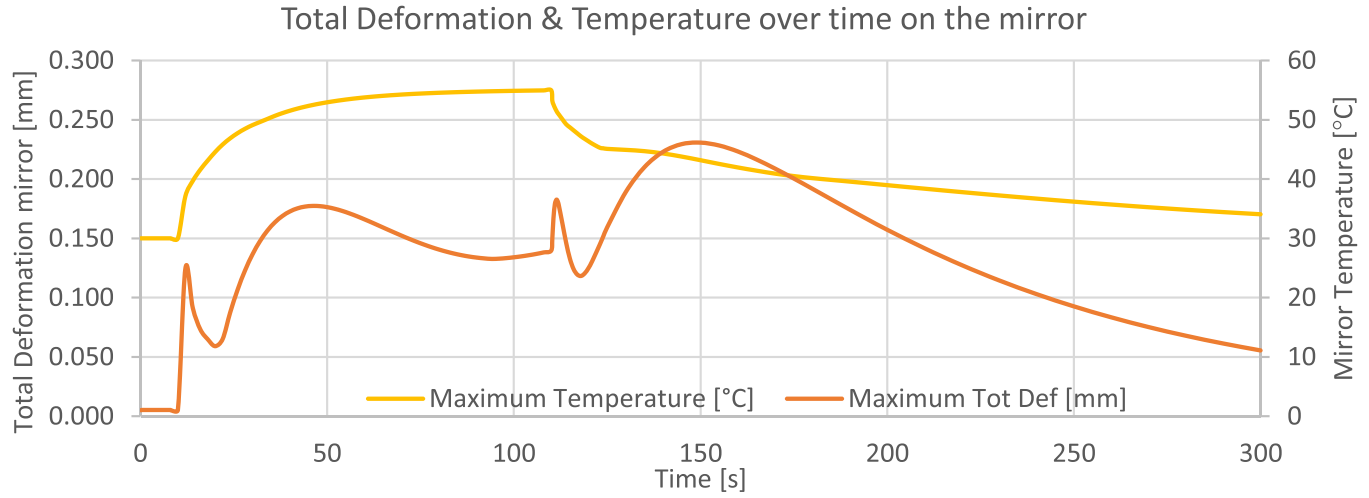


**Fig. 27.** Maximum total deformation and temperature over time in the last version of the copper mirror.

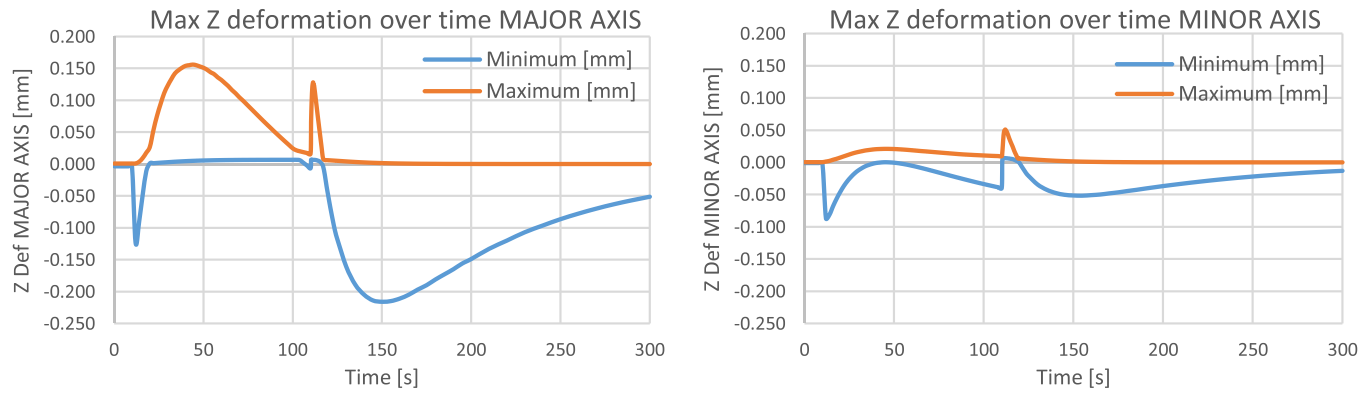


**Fig. 28.** Minimum and maximum Z-deformation along the major (left) and minor (right) axes in the last version of the copper mirror.

time, with an increase in water temperature of 13.8 °C and 18.5 °C in the internal and external channels, respectively.

The thermal gradient along the radius and especially across the thickness results in thermal expansion effects. At the end of the pulse, the maximum total deformation is 0.140 mm. Despite the maximum temperatures are registered at the end, the most critical instant from the deformation point of view is approximately 34 s after the start of the pulse, when the maximum total deformation reaches a value of 0.177 mm. Even the first instants could be dangerous, because a sudden increase in deformation occurs about 1.5 s after the start of the pulse, producing deformation in the opposite direction (negative deformation in the Z-direction). However, the maximum value is lower than the one at 34 s and more abrupt. If the deformation at 34 s will be acceptable, it will not be necessary to further analyse the deformations occurring at later times.

The resulting deformed geometry at the critical instant will be verified with electromagnetic codes to study its effect on the beams' propagation.

## CRediT authorship contribution statement

**A. Salvitti:** Conceptualization, Methodology, Software, Data curation, Formal analysis, Writing – original draft, Writing – review & editing, Visualization. **A. Bruschi:** Conceptualization, Validation, Resources, Supervision, Writing – review & editing. **G. Calabrò:** Supervision, Validation, Funding acquisition. **F. Fanale:** Conceptualization, Investigation, Resources, Writing – review & editing. **P. Fanelli:** Supervision, Conceptualization, Methodology, Validation, Writing – original draft, Funding acquisition. **S. Garavaglia:** Resources, Writing – review & editing, Visualization. **F. Giorgetti:** Conceptualization, Methodology, Software, Formal analysis, Writing – original draft, Visualization. **G. Granucci:** Project administration, Supervision. **A. Moro:** Conceptualization, Investigation, Resources, Supervision, Writing – review & editing. **P. Platania:** Formal analysis. **A. Romano:** Project administration, Writing – review & editing.

## Declaration of competing interest

The authors declare that they have no known competing financial interests or personal relationships that could have appeared to influence the work reported in this paper.

## Data availability

The data that has been used is confidential.

## Acknowledgment

This work is carried out in the frame of the DTT activity. The authors are very grateful to all the colleagues involved in the DTT project for their precious contributions.

## References

[1] DTT divertor tokamak test facility interim report (2023)- http://www.enea.it/en/publications/abstract/DTT-Divertor-Tokamak-Test-facility-Interim-Design-Report.
[2] G. Federici, et al., Overview of the DEMO staged design approach in Europe, Nucl. Fusion. 59 (2019), 066013.
[3] G. Granucci, et al., The DTT device: system for heating, Fusion Eng. Des. 122 (2017) 349–355.
[4] S. Ceccuzzi, et al., Conceptual definition of an ICRF system for the Italian DTT, Fusion Eng. Des. 146 (2019) 361–364.
[5] P. Agostinetti, et al., Conceptual design of a neutral beam heating & current drive system for DTT, Fusion Eng. Des. 146 (2019) 441–446.
[6] S. Garavaglia, et al., Preliminary conceptual design of the DTT EC heating system, Fusion Eng. Des. 146 (2019) 203–206.
[7] L. Empacher, W. Kasparek, Analysis of a multiple-beam waveguide for free-space transmission of microwaves, IEEE Trans. Antennas Propag. 49 (3) (Mar. 2001) 483–493.
[8] V. Erckmann, et al., ECRH for W7-X: transmission losses of high-power 140 GHz wave beams, Fusion Sci. Technol. 55 (1) (2009) 16–22.
[9] S. Garavaglia, et al., Progress of DTT ECRH system design, Fusion Eng. Des. 168 (2021), 112678.
[10] A. Bruschi, et al., Conceptual design of the DTT ECRH quasi-optical transmission line, Fusion Eng. Des. 194 (2023), 113727.
[11] P.F. Goldsmith, Quasioptical Systems, IEEE Press, 1998. ISBN 0780334396.
[12] Kasparek, et al., Measurements of ohmic losses of metallic reflectors at 140 GHz using a 3-mirror resonator technique, Int. J. Infrared Millim. Waves 22 (2001) 1695–1707.
[13] A. Salvitti, et al., Preliminary design and thermal analyses of the steerable mirror cooling channel of the DTT ECRH, Fusion Eng. Des. 161 (2020), 111880.
[14] ANSYS, Inc, Mechanical User's Guide, Release 18.2, Canonsburg, 2017.
[15] V. Erckmann, et al., Electron cyclotron heating for W7-X: physics and technology, Fusion Sci. Technol. 52 (2) (2007) 291–312.
[16] W. Kasparek, et al., Mirror development for the 140 GHz ECRH transmission system on the stellarator W7-X, Fusion engineering and design 53 (1-4) (2001) 545–551, https://doi.org/10.1016/S0920-3796(00)00532-9.
[17] H. Hailer, et al., Mirror development for the 140 GHz ECRH system of the stellarator W7-X, Fusion Eng. Des. 66 (2003) 639–644.